Article

Mineralogy and Metallogenesis of the Sanbao Mn–Ag (Zn-Pb) Deposit in the Laojunshan Ore District, SE Yunnan Province, China

Shengjiang Du [1,2], Hanjie Wen [3,4,*], Shirong Liu [3], Chaojian Qin [3], Yongfeng Yan [5], Guangshu Yang [5] and Pengyu Feng [5]

1   State Key Laboratory of Nuclear Resources and Environment, East China University of Technology, Nanchang 330013, China; shengjiangdu@163.com
2   Chinese Academy of Geological Science, Beijing 100037, China
3   State Key Laboratory of Ore Deposit Geochemistry, Institute of Geochemistry, Chinese Academy of Sciences, Guiyang 550081, China; liushirong@vip.gyig.ac.cn (S.L.); qinchaojian@vip.skleg.cn (C.Q.)
4   University of Chinese Academy of Sciences, Beijing 100049, China
5   Kunming University of Science and Technology, Kunming 650093, China; yyf701018@sina.com (Y.Y.); 13888600582@163.com (G.Y.); rockfpy@163.com (P.F.)
*   Correspondence: wenhanjie@vip.gyig.ac.cn

Abstract: The Sanbao Mn–Ag (Zn-Pb) deposit located in the Laojunshan ore district is one of the most important deposits that has produced most Ag and Mn metals in southeastern Yunnan Province, China. Few studies are available concerning the distribution and mineralization of Ag, restricting further resource exploration. In this study, detailed mineralogy, chronology, and geochemistry are examined with the aim of revealing Ag occurrence and its associated primary base-metal and supergene mineralization. Results show that manganite and romanèchite are the major Ag-bearing minerals. Cassiterite from the Mn–Ag ores yielded a U–Pb age of 436 ± 17 Ma, consistent with the Caledonian age of the Nanwenhe granitic pluton. Combined with other geochemical proxies (Zn-Pb-Cu-Sn), the Sanbao Mn–Ag deposit may originally be of magmatic hydrothermal origin, rather than sedimentary. The Ag-rich (Zn-Pb (Sn)-bearing) ore-forming fluids generated during the intrusion of the granite flowed through fractures and overprinted the earlier Mn mineralization. Secondary Ag (and possibly other base-metals) enrichment occurred through later supergene weathering and oxidation.

Keywords: the Sanbao Mn–Ag deposit; manganite; romanèchite; rhodochrosite; Caledonian granitic pluton; China

1. Introduction

Mn–Ag deposits are among the most important types of silver deposits in China. It is difficult to separate Ag from manganese–silver ores due to a lack of research into the occurrence state (form) of silver and a lack of metallogenic models [1–6]. Research on mineralogy and metallogenesis is helpful to illuminate the existing state of silver and establish the actual metallogenetic model of these Mn–Ag deposits. Furthermore, there are four main types of silver occurrence state [1,7], namely, independent silver minerals, the isomorphic state, ionic adsorption, and the amorphous state.

Mn and Ag are the dominant metals produced in the Sanbao deposit. The Sanbao Mn–Ag deposit, located in the Laojunshan ore district in the southeast of the Yunnan Province of China, is one of the important Mn and Ag metal resources in southwestern China. In addition to Mn, this deposit is characterized by Ag enrichment with a mean value of 221 ppm and special Ag-bearing minerals.

The metallogenetic model of the Sanbao Mn–Ag deposit remains in dispute and research about the existing state of silver is almost non-existent. Jia [8] considered that the Sanbao Mn–Ag deposit has obvious stratabound characteristics and features of volcanic exhalation–sedimentation as well as of distal skarns. Part of the ore body is formed in interlayer fracture zones. The contact zone between marble and schist should be conducive to ore fluid precipitation. Yang et al. [9] indicated that the Middle Cambrian Tianpeng Formation, with high background values of ore-forming elements, provides the repository for all ores and protores. The Sanbao Mn–Ag deposit is strictly controlled by the Tianpeng Formation and the main ore features a banded structure. In the course of its creation and evolution, the Mn–Ag ore formed through activation, migration, and concentration of Mn and Ag caused by the multiple-epoch metamorphism of the source bed. Although the geology and geochemistry of the Sanbao Mn–Ag deposit are available [8,10], the origin of this deposit is still poorly understood.

The study of these Ag occurrences could play an important role in presenting a genetic model for the source and formation of ore-forming materials. The hosting mineralogy and its enrichment are poorly constrained in the Sanbao deposit. From a detailed study of Ag-bearing minerals and chronology, we propose a new genetic model for this deposit. In this study, the results of electron probe microanalysis (EPMA) confirmed that Ag exists mainly in manganite and romanèchite in the state of isomorphism. It is important for a mining company to select a proper mineral processing procedure to recover silver. Additionally, based on the isotopic geochronology and the spatial distribution of industrial orebodies, the genesis of the Sanbao manganese–silver deposit was studied, and a mineralization model established to provide information for future prospecting in the broad region.

2. Geological Background

The South China Craton consists of the Yangtze Block to the northwest and the Cathaysia Block to the southeast (Figure 1a) [11,12]. The South China Craton was welded to the North China Craton to the north and the Indochina Block to the south during the Triassic [13–15]. The Yangtze and Cathaysia blocks were amalgamated along the Jiangnan Fold Belt at around 830 Ma (Neoproterozoic time) in South China [11,15]. Large-scale mineralization in these two blocks occurred from the Proterozoic to the Cenozoic, making the region one of the most important polymetallic metallogenic provinces in the world. The basement of the Yangtze Block consists mainly of late Archean metamorphic rocks in the north and late Paleo to Neoproterozoic weak metamorphosed rocks in the west and east, all of which were intruded by Neoproterozoic igneous rocks [16,17]. The sedimentary succession of the Yangtze Block is mainly composed of Cambrian to Triassic marine sedimentary rocks and Jurassic–Cretaceous and Cenozoic continental sedimentary rocks [18]. The Cathaysia Block is characterized by widespread, 1.9–1.8-Ga, Neoproterozoic to Early Paleozoic metamorphic rocks [19]. In particular, there are widespread igneous intrusions with ages ranging from 480 to 400 Ma, 230 to 200 Ma, and 100 to 80 Ma [19]. Widespread polymetallic mineralization is spatially and temporally associated with the above tectonic-thermal events and igneous activities in South China.

The Laojunshan ore district is located in the southeast of Yunnan Province (southwest China) and occupies the junction of the Yangtze Block to the north and the Cathaysia Block in the east. Several Yanshanian igneous intrusions were emplaced roughly along the juncture of the Yangtze Block and the Cathaysia Block, including the Gejiu, Bozhushan, and Laojunshan intrusions [20,21]. A series of super-large ore deposits (e.g., the Gejiu Sn deposit, the Bainiuchang Ag-polymetallic deposit, and the Dulong Sn–Zn–In polymetallic deposits [22]) are closely related to these igneous activities, forming one of the most important polymetallic tungsten–tin mineralized belts in China. The Laojunshan granite itself is surrounded by a number of large ore deposits, such as the Sanbao Mn–Ag deposit, the Xinzhai Sn deposit, the Nanyangtian W deposit, and the Dulong Sn–Zn–In polymetallic deposits (Figure 1b). These deposits constitute a large polymetallic Sn–W–Pb–Zn–Cu ore district [23], also known as the Laojunshan ore district.
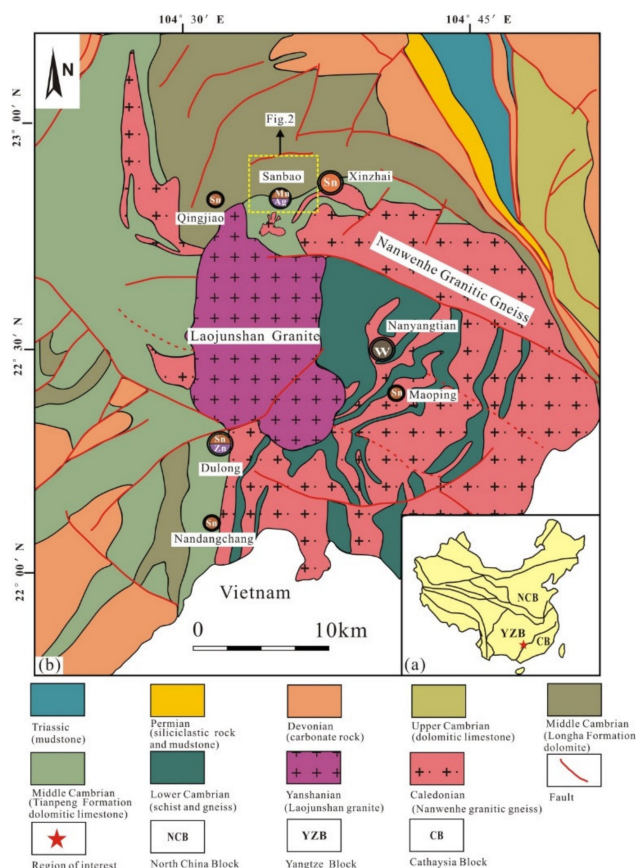
Figure 1. (**a**) The tectonic location of the Laojunshan ore district and (**b**) its geologic map (modified from [20]).

Two types of granites occur in the Laojunshan ore district: one is Laojunshan granite formed in the Yanshanian and another is Nanwenhe granitic gneiss formed in the Caledonian. The Nanwenhe granitic gneiss is located mainly in the eastern part of the Laojunshan granite body. The Nanwenhe granitic gneiss is close to a deformed and metamorphosed dome, the Laojunshan-Song Chay Dome [18]. The Laojunshan Metamorphic Core Complex and Song Chay metamorphic dome extend from the belt between the NW–SE trending Wenshan–Malip fault zone and NW–SE striking Red River shear zone. The dome is the largest in the southwestern part of the South China Block and extends into Vietnam [8]. The so-called "Nanwenhe granitic gneiss" is composed of light gray intermediate to fine-grained granite with a porphyritic texture and gneissic fabric. The Nanwenhe granitic gneiss was metamorphosed or deformed into gneissic granite and granite gneiss in the Triassic. Porphyritic texture and gneissic fabric are found in the Nanwenhe granitic gneiss. Furthermore, these rocks can be further subdivided petrographically into the Tuantian and Laochengpo units [20]. Both have similar mineral assemblages, including quartz, feldspar, and mica, with minor sulfides and zircon.

The Sanbao Mn–Ag deposit occurs at the north margin of the Laojunshan ore district (Figure 1b). Drilling identified potentially ore grade materials, including 13.2% Mn and 221 g/t Ag in this deposit. This deposit has an estimated 200 tons of Ag reserves and 15,000 tons of Mn reserves. It is considered to be a medium-sized reserve and is potentially expected to become a large-scale deposit. The main faults trend NW and NE and dip at a relatively high angle to the east in the Sanbao deposit (Figures 2a and 3a). Mn–Ag orebody distribution was strictly controlled by the main faults (Figure 2a). Outcrops rocks include Middle Cambrian metamorphic rock series, carbonate rocks, and granite associated with the Yanshanian and Caledonian magmatism in the Laojunshan ore district [8,10,20,24]. The Middle Cambrian Tianpeng Formation is the dominant host for mineralization. It can be sub-divided into five units: unit 1 is chiefly composed of quartz schist and skarn; unit 2 consists of dolomitic marble and

minor skarn; unit 3 consists of quartz schist with subordinate mica schist; unit 4 is composed of mica schist, limestone, and dolomitic limestone; and unit 5 consists of mica schist and quartz schist (Table 1). The Mn–Ag orebodies are mainly hosted in unit 4 and unit 5. The Tianpeng Formation is overlain by the Longha Formation.
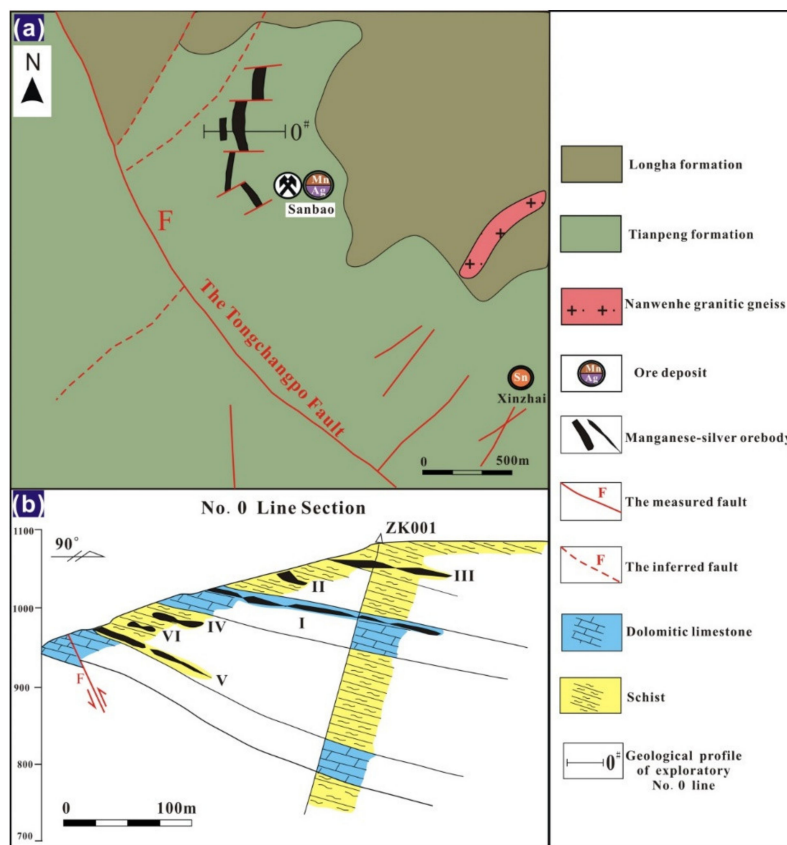

Figure 2. (**a**) Simplified geologic map of the Sanbao Mn–Ag deposit; and (**b**) cross-section of exploration line 0 (modified from [8]).

Table 1. Details of the Tianpeng Formation from the Sanbao deposit.

Layer No.	Thickness (m)	Lithology	Mineralization
Fifth (Unit 5)	244	Mica schist and quartz schist	Good
Fourth (Unit 4)	28–154	Mica schist, limestone and dolomitic limestone	Better
Third (Unit 3)	250	Quartz schist with subordinate mica schist	Poor
Second (Unit 2)	70–298	Dolomitic marble and some skarn	Poor
First (Unit 1)	235	Quartz schist and skarn	Poor

The Sanbao Mn–Ag deposit is comprised of primarily stratabound, lenticular, capsular, and irregular orebodies (Figure 2b). The Sanbao deposit primarily consists of six mineralized belts with 29 orebodies. The no. 1 ore body is the most important in the deposit. It consists of 12 small orebodies and is primarily hosted in the limestone of the Tianpeng Formation unit 4.

The wall rock alteration includes silicification (Figure 3b), lead–zinc mineralization, pyritization (Figure 3c), and skarnification (Figure 3d). Silicification is developed in most Tianpeng units that are composed of quartz schist. Lead–zinc mineralization and pyritization occur in the wall rock; for example, galena, sphalerite, and pyrite are formed within the mica schist. Skarnification occurs mainly in the wall rock, termed skarn, which is not far from the Mn–Ag ore body. The skarn is mainly composed of assemblages containing diopside and tremolite in the Sanbao area.

Figure 3. Photographs of the Mn–Ag orebodies in the Sanbao deposit: (**a**) contact relationship between Mn–Ag orebodies and the fault; (**b**) quartz vein cut through the quartz schist; (**c**) lead–zinc mineralization in wall rock; (**d**) skarn alteration; (**e**) some rhodochrosite was distributed by vein in limestone; (**f**) fracture developed in the primary rhodochrosite and fracture filled with calcite.

3. Samples and Analytical Methods

There are three types of ores in the Sanbao deposit: primary, partial oxidized, and strongly oxidized ores. Samples for this study were collected from the three types of ores (Figures 3–5). The primary ore, made up largely of rhodochrosite (Figure 3e), has little Ag and is characterized by a dense texture (Figure 4a). Additionally, the primary ore contains calcite veins and sulfide minerals, such as pyrite and chalcopyrite (Figure 3f, Figure 4b,c). The partial oxidized ore with porous texture is mainly composed of limonite, pyrolusite, and minor amounts of manganite and romanèchite (Figure 4d,e). The strong oxidized ore mainly consists of manganite, romanèchite, pyrolusite, and a small amount of limonite. The strong oxidized ore showed an unconsolidated and powdery texture (Figure 4f). We carried out electron probe microanalysis (EPMA) and inductively coupled plasma–mass spectrometry (ICP-MS) for trace elements analysis, and laser ablation–multicollector–inductively coupled plasma–mass spectrometry (LA-MC-ICP-MS) cassiterite U–Pb dating was also conducted.
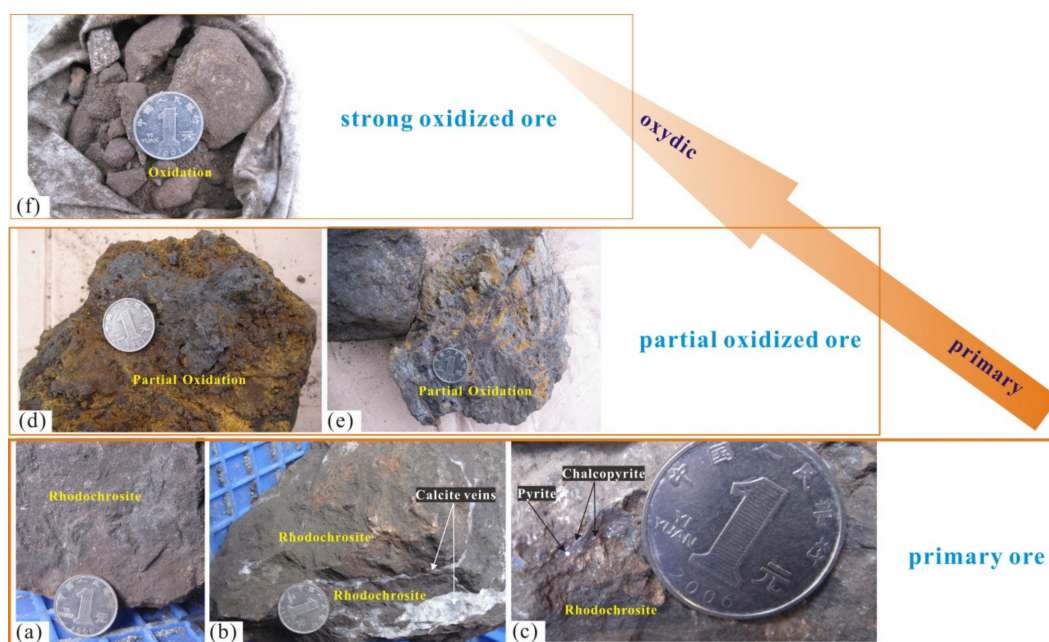
Figure 4. Specimens of Mn–Ag ore from the Sanbao deposit: (**a**) rhodochrosite is the main mineral composition of pre-ore (primary ore); (**b**) typical vein structure in rhodochrosite; (**c**) pyritization with chalcopyrite in rhodochrosite; (**d**) partial oxidized syn-ore mainly is composed of diopside and has a porous texture; (**e**) there are many pores (voids), even cracks, and loose texture in partial oxidized syn-ore; (**f**) unconsolidated and powdery texture in the post-ore (strong oxidized-ore).
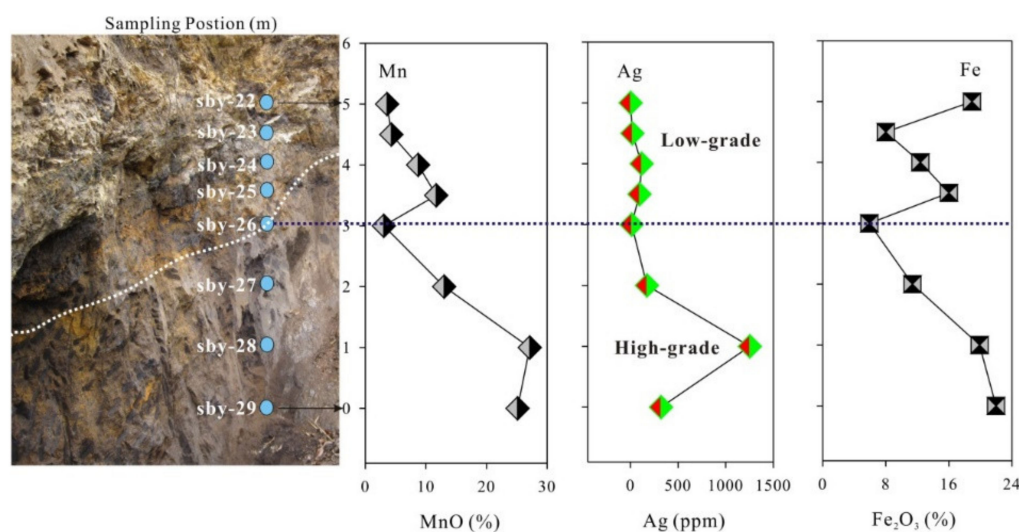
Figure 5. Elemental variation within a vertical profile from the Sanbao deposit.

3.1. EPMA

Mineralogical observations for Mn and Ag were performed using a Shimadzu EPMA-1600 electron microprobe equipped with an energy-dispersive spectrometer and back-scatter electron (BSE) imaging capability at the State Key Laboratory of Ore Geochemistry of the Institute of Geochemistry, Chinese Academy of Sciences (IGCAS, Guiyang, China). SPI (Structure Probe Incorporation) standards were used, and the minimum detection limits of Mn, Ag, Fe, Ba, K, Zn, Ca, Si, Cr, Al, Ti, Na, and Sr were 0.1%. The selected analytical spectral lines and deducted background values were achieved using instrument programs, and some fault spectral peaks were calibrated artificially. In addition, a JEM-2000FX II TEM with an Oxford Link ISIS energy dispersive X-ray spectrometer (EDS) was also

used to observe the texture and size of the Ag-bearing minerals at the IGCAS. All data are given in terms of weight percent (wt.%).

3.2. Trace Elements Analysis

Trace elements were analyzed using a Perkin-Elmer Sciex ELAN 6000 ICP-MS at the IGCAS. The powdered samples (50 mg) were dissolved in high-pressure Teflon bombs using a HF + HNO_3 mixture for 48 h at 190 °C [25]. Rh was used as an internal standard to monitor signal drift during counting. The GBPG-1 (Garnet-Biotite Plagiogneiss) international standard was used for analytical quality control. Analyses of the OU-6 (Penrhyn Slate) and GBPG-1 international standards agreed with the recommended values and the analytical precision was generally better than 5% for all elements [26].

3.3. LA-MC-ICP-MS Cassiterite U–Pb Dating

LA-MC-ICP-MS cassiterite U–Pb analyses were carried out at the Tianjin Institute of Geology and Mineral Resources, Tianjin, China. In-situ LA-MC-ICP-MS U–Pb dating of cassiterite from the Mn–Ag ore was used to determine the geochronology. More information about the instrumental parameters and operating conditions can be found in previous research [23,27–30]. For the cassiterite sample, we used the correction value (K = measured value (164)/"true value" (158)) of 0.96 calculated using the external standard (AY-4) to correct the deviations between the measured and "true" isotopic ratios. The $^{207}Pb/^{206}Pb$ and $^{238}U/^{206}Pb$ ratios were corrected using the cassiterite external standard, and the calculated ages were determined using Isoplot software [31].

4. Results

Two samples (sby-28 and sby-03) were selected for EPMA analysis. The EPMA results show that the main Ag-bearing minerals are manganite and romanèchite. Results of manganite and romanèchite from electron probe X-ray microanalysis are listed in Tables 2 and 3.

The Ag, trace element, and REE (Rare Earth Elements) compositions are reported in Tables 4 and 5. The oxidized ores contain higher amounts of Ag (1.42–1253 ppm) than the pure rhodochrosite ones (Ag: 8.3–91.4 ppm). The wall rocks are characterized by low Ag (1.41–1.69 ppm) concentrations compared with the ores. The ores have strongly positive Eu anomalies, but the wall rocks have no abnormalities.

Table 2. Electron probe X-ray microanalysis (wt.%) of acicular manganite from the Sanbao deposit.

Spot No.	Al_2O_3	TiO_2	Cr_2O_3	MnO	FeO	K_2O	Ag_2O	ZnO	SiO_2	CaO	Total	Calculated Formula
sby-28-9	n.d.	n.d.	0.20	71.79	4.29	1.12	0.50	0.66	n.d.	0.14	78.70	$(Mn_{0.91}Fe_{0.05}K_{0.02}Zn_{0.01})_{0.99}O(OH)$
sby-28-10	n.d.	n.d.	0.10	69.21	4.75	1.06	0.45	0.66	n.d.	0.17	76.40	$(Mn_{0.90}Fe_{0.06}K_{0.02}Zn_{0.01})_{0.99}O(OH)$
sby-28-11	0.32	0.21	0.64	71.07	4.57	1.13	0.57	0.68	0.36	0.21	79.76	$(Mn_{0.89}Fe_{0.06}K_{0.02}Zn_{0.01})_{0.98}OOH$
sby-28-12	0.44	n.d.	0.38	73.22	4.14	1.16	0.51	0.63	0.10	0.26	80.84	$(Mn_{0.90}Fe_{0.05}K_{0.02}Zn_{0.01})_{0.98}OOH$
sby-28-13	0.49	n.d.	0.21	72.78	4.45	1.16	0.56	0.72	n.d.	0.37	80.74	$(Mn_{0.90}Fe_{0.05}K_{0.02}Zn_{0.01})_{0.98}OOH$
sby-28-14	n.d.	n.d.	0.17	70.17	3.99	1.17	0.62	0.71	n.d.	0.18	77.01	$(Mn_{0.91}Fe_{0.05}K_{0.02}Zn_{0.01})_{0.99}OOH$
sby-28-15	n.d.	n.d.	0.11	71.36	4.73	1.02	0.47	0.72	0.10	0.13	78.64	$(Mn_{0.91}Fe_{0.06}K_{0.02}Zn_{0.01})_{1.00}OOH$
sby-28-16	n.d.	n.d.	0.32	69.32	5.66	0.97	0.51	0.65	n.d.	0.13	77.56	$(Mn_{0.89}Fe_{0.07}K_{0.02}Zn_{0.01})_{0.99}OOH$
sby-28-17	0.1	n.d.	0.03	72.69	4.99	1.09	0.54	0.71	n.d.	0.12	80.27	$(Mn_{0.90}Fe_{0.06}K_{0.02}Zn_{0.01})_{0.99}OOH$
sby-28-18	0.67	n.d.	0.25	72.21	4.63	1.01	0.51	1.03	0.15	0.28	80.74	$(Mn_{0.89}Fe_{0.06}K_{0.02}Zn_{0.01})_{0.98}OOH$
Mean	0.21	n.d.	0.24	71.38	4.62	1.09	0.52	0.72	0.10	0.20	79.08	$(Mn_{0.90}Fe_{0.06}K_{0.02}Zn_{0.01})_{0.99}OOH$

Table 3. Electron probe X-ray microanalysis (wt.%) of massive romanèchite from the Sanbao deposit.

Spot No.	Al_2O_3	MnO	FeO	Ag_2O	ZnO	CaO	BaO	SrO	Na_2O	K_2O	Total	Calculated Formula
sby-03-3	0.48	63.36	7.44	2.83	0.82	n.d.	7.72	n.d.	n.d.	0.70	83.35	$(Ba_{0.26}Ag_{0.13}K_{0.08}Fe_{0.03}(H_2O)_{1.50})_{\Sigma2.00}(Mn_{0.45}Zn_{0.05}Mn_{3.94}Fe_{0.51}Al_{0.05})_{\Sigma5.00}O_{10}$
sby-03-4	0.58	60.19	10.54	1.87	0.73	n.d.	8.19	n.d.	n.d.	0.55	82.65	$(Ba_{0.23}Ag_{0.08}K_{0.06}Fe_{0.09}(H_2O)_{1.50})_{\Sigma1.96}(Mn_{0.46}Zn_{0.05}Mn_{3.79}Fe_{0.65}Al_{0.06})_{\Sigma5.19}O_{10}$
sby-03-5	1.22	55.36	15.21	0.21	0.98	0.10	4.30	n.d.	0.34	0.43	78.15	$(Ba_{0.14}Ag_{0.01}K_{0.04}Na_{0.05}Fe_{0.25}(H_2O)_{1.50})_{\Sigma1.99}(Mn_{0.44}Zn_{0.06}Mn_{3.62}Fe_{0.77}Al_{0.12})_{\Sigma5.01}O_{10}$
sby-03-6	0.55	60.86	11.01	1.55	0.92	0.10	7.21	n.d.	0.10	0.45	82.75	$(Ba_{0.12}Ag_{0.03}K_{0.03}Fe_{0.11}(H_2O)_{1.50})_{\Sigma1.79}(Mn_{0.44}Zn_{0.06}Mn_{3.81}Fe_{0.63}Al_{0.06})_{\Sigma5.00}O_{10}$
sby-03-7	0.61	57.88	11.44	1.44	0.89	n.d.	6.53	n.d.	0.10	0.43	79.32	$(Ba_{0.21}Ag_{0.06}K_{0.05}Fe_{0.12}(H_2O)_{1.50})_{\Sigma1.94}(Mn_{0.45}Zn_{0.06}Mn_{3.80}Fe_{0.64}Al_{0.06})_{\Sigma5.01}O_{10}$
sby-03-9	1.07	61.08	6.40	0.04	5.41	n.d.	1.06	n.d.	0.20	0.42	75.68	$(Ba_{0.04}K_{0.05}Fe_{0.38}(H_2O)_{1.50})_{\Sigma1.97}(Mn_{0.15}Zn_{0.35}Mn_{4.30}Fe_{0.09}Al_{0.11})_{\Sigma5.00}O_{10}$
sby-03-10a	2.21	64.80	6.44	0.26	1.14	0.10	4.11	0.11	0.11	0.75	80.03	$(Ba_{0.14}Ag_{0.01}K_{0.08}Fe_{0.23}(H_2O)_{1.50})_{\Sigma1.96}(Mn_{0.43}Zn_{0.07}Mn_{4.03}Fe_{0.24}Al_{0.23})_{\Sigma5.00}O_{10}$
sby-03-10b	2.01	65.73	6.09	0.19	1.33	0.12	3.60	n.d.	0.20	0.90	80.17	$(Ba_{0.13}Ag_{0.01}K_{0.10}Fe_{0.22}(H_2O)_{1.50})_{\Sigma1.96}(Mn_{0.41}Zn_{0.07}Mn_{4.06}Fe_{0.23}Al_{0.21})_{\Sigma4.98}O_{10}$
sby-03-10c	3.70	60.57	6.47	0.18	1.75	0.06	3.44	n.d.	0.13	1.11	77.41	$(Ba_{0.11}Ag_{0.01}K_{0.12}Fe_{0.23}(H_2O)_{1.50})_{\Sigma1.97}(Mn_{0.39}Zn_{0.11}Mn_{3.90}Fe_{0.22}Al_{0.37})_{\Sigma4.99}O_{10}$
sby-03-11	0.55	59.94	8.95	2.47	1.17	0.12	6.59	n.d.	0.10	0.61	80.50	$(Ba_{0.22}Ag_{0.11}K_{0.07}Fe_{0.08}(H_2O)_{1.50})_{\Sigma1.98}(Mn_{0.43}Zn_{0.07}Mn_{3.89}Fe_{0.56}Al_{0.06})_{\Sigma5.01}O_{10}$
Mean	1.30	60.97	9.00	1.10	1.51	0.10	5.27	n.d.	0.12	0.63	80.00	$(Ba_{0.18}Ag_{0.05}K_{0.07}Fe_{0.18}(H_2O)_{1.50})_{\Sigma1.98}(Mn_{0.41}Zn_{0.10}Mn_{3.91}Fe_{0.46}Al_{0.13})_{\Sigma4.74}O_{10}$

Table 4. Silver and trace element contents (ppm) of the oxidized ores, primary ores (pure rhodochrosite), and wall rocks from the Sanbao deposit.

Sample No.	Lithology	Ag	Li	V	Cr	Co	Ni	Cu	As	Sr	Zr	Nb	Mo	Sb	Cs	Ba	W	Ti	Pb	Th	U	Zn
sby-01	Oxidized ore	261	14.5	23	78	3.7	73.8	91.1	375	80.8	11.4	0.8	0.82	66.9	20.9	290	4.0	0.029	17,540	4	1.9	16,520
sby-02	Oxidized ore	530	6.9	2	19	1	24.6	35.8	125.5	153	3.9	0.4	0.52	28.1	10.6	20	2.1	0.005	9450	0.5	1	8910
sby-03	Oxidized ore	806	1.6	1	48	0.6	14.5	153.5	216	243	3.9	0.5	0.45	97.5	9.92	10	2.3	0.005	18,750	0.4	1	17,660
sby-06	Oxidized ore	98.7	224	68	68	807	153.5	186.5	126.5	171	21.3	1.6	3.79	66	2.9	5700	2.9	0.075	2240	10.4	7.5	2110
sby-16	Oxidized ore	65.3	18.2	31	42	9.2	30.0	22.4	2790	184	16.7	1.0	0.51	867	23.9	140	1.9	0.044	3510	7.6	1.3	4960
sby-22	Oxidized ore	1.42	333	136	158	90.6	452	81.2	73.5	82.6	50.3	5.1	1.92	36.9	14.95	470	7.5	0.184	2210	28.9	6.1	1430
sby-23	Oxidized ore	19	142.5	23	149	123.5	154.5	197	179.5	19.3	8.8	1.1	1.3	133.5	5.07	660	3.4	0.034	5360	5.4	3.2	5240
sby-24	Oxidized ore	116	47.1	14	272	204	68.1	405	301	21.7	4.1	0.5	1.6	294	4.55	2690	3.0	0.012	8140	2.9	4.9	7630
sby-25	Oxidized ore	94.6	112	32	372	232	179.5	434	422	28.9	15	1.1	1.8	264	7.31	2890	4.5	0.04	8590	7	6.3	8100
sby-26	Oxidized ore	12.45	107.5	80	90	87.2	163	143	974	33.2	58.5	4.4	0.63	47.8	14.2	890	6.9	0.193	4000	36.1	3.1	1650
sby-27	Oxidized ore	173	58	59	90	19.6	242	469	1340	52.1	33	1.6	2.29	131	14.5	3840	7.8	0.108	6480	14.7	5.1	7660
sby-28	Oxidized ore	1253	18	22	98	2.6	231	124	1750	81.1	8.3	0.6	7.71	173.5	10.8	25,020	21.3	0.015	5800	2.8	7.8	6180
sby-29	Oxidized ore	321	17.7	19	137	2.0	138.5	68.7	1290	68.3	7.0	0.6	2.61	154.5	26.0	3520	3.0	0.012	4170	2	3.9	9790
sbyd-10	Pure rhodochrosite	91.4	0.4	<1	<1	3.2	4.5	108.5	744	196	7.1	0.7	0.26	299	0.85	40	1.2	<0.005	51,880	0.7	1.8	48,670
sbyd-12	Pure rhodochrosite	55.1	0.6	<1	<1	2.5	6.3	180	594	48.7	3.0	0.8	0.08	44.9	0.31	<10	1.4	<0.005	6000	0.3	0.7	35,310
sbyd-14	Pure rhodochrosite	43.1	0.5	<1	3	2.9	6.4	152	484	83.2	11.1	0.4	1.21	54.4	0.18	70	8.7	<0.005	52,230	0.4	1.8	48,970
sbyd-20	Pure rhodochrosite	32.5	1.4	<1	<1	2.8	4.1	203	193.5	96.1	5.2	0.7	0.3	11.4	0.88	10	5.2	<0.005	1980	0.3	0.7	12,170
2sby-3	Pure rhodochrosite	8.3	1.5	<1	<1	1.4	1.4	56.7	294	154.5	6.1	0.9	0.51	6.97	1.04	20	0.5	<0.005	3860	0.2	0.8	24,240
sby-12	Wall rock	1.69	34.4	97	83	22	57.7	57.1	17.9	183.5	24.6	10.1	0.34	0.74	6.41	420	3.0	0.325	51.9	18.1	2.3	187
sby-13	Wall rock	1.41	3.2	8	9	4.6	6.7	7.1	8	615	8.9	1	0.8	2.64	0.87	70	1.0	0.026	111.5	5.1	1.8	173

Table 5. REE (ppm) composition of the pure rhodochrosite (primary ore) and wall rocks from the Sanbao deposit.

Sample No. Lithology	sbyd-10	sbyd-12	sbyd-14	sbyd-20	2SBY-3	sby-12	sby-13
			Pure Rhodochrosite			Wall Rock	
La	8.1	12.4	10.6	11.2	8.3	31.9	7.9
Ce	15.25	21.4	20.9	16.5	15.15	79.8	20.3
Pr	1.46	2.2	1.5	1.73	1.67	8.43	2.03
Nd	5.1	8.0	4.9	5.8	6.0	31.1	7.9
Sm	0.93	1.43	0.82	0.93	1.1	5.63	1.54
Eu	1.22	1.56	2.32	1.46	1.06	1.06	0.34
Gd	1.1	1.19	0.97	0.76	0.94	4.95	1.41
Tb	0.14	0.13	0.11	0.09	0.11	0.73	0.21
Dy	0.66	0.68	0.56	0.45	0.55	4.15	1.19
Ho	0.12	0.13	0.11	0.09	0.1	0.82	0.24
Er	0.32	0.32	0.31	0.24	0.26	2.24	0.68
Tm	0.05	0.05	0.05	0.03	0.03	0.3	0.1
Yb	0.3	0.29	0.29	0.19	0.21	1.82	0.63
Lu	0.05	0.05	0.05	0.04	0.03	0.25	0.1
Y	4.8	6.4	4.3	3.9	4.8	22	9.1
ΣREE	34.8	49.83	43.49	39.51	35.51	173.18	44.57
LREE(light rare earth elements)	32.06	46.99	41.04	37.62	33.28	157.92	40.01
HREE(heavy rare earth elements)	2.74	2.84	2.45	1.89	2.23	15.26	4.56
LREE/HREE	11.7	16.55	16.75	19.9	14.92	10.35	8.77
LaN/YbN	2.55	4.03	3.45	5.56	3.73	1.65	1.18
δEu	5.6	5.61	12.08	8.15	4.89	0.94	1.08
δCe	1.04	0.96	1.19	0.86	0.96	1.15	1.2

The cassiterite from the Sanbao Mn–Ag ores is light to dark brown, mostly euhedral to subhedral under the observation of an optical microscope. The U–Pb data for the cassiterite (sby-03) are summarized in Table 6. The external standard (AY-4) yielded an isochron age of 164 ± 12 Ma, which is consistent with the "standard" age of 158.2 ± 0.4 Ma, within the margin of error. The cassiterite sample (sby-03) yielded an isochron age of 436 ± 17 Ma.

Table 6. U–Pb isotopic data for cassiterite (sby-03 from the Sanbao deposit; AY-4 in-house external standard).

sby-03	$^{238}U/^{206}Pb$	2σ (%)	$^{207}Pb/^{206}Pb$	2σ (%)	$^{238}U/^{206}Pb$	2σ (%)	$^{207}Pb/^{206}Pb$	2σ (%)
	4.22	4.5	0.5878	6.7	11.58	3.7	0.1652	17.3
	2.40	4.6	0.7087	4.1	10.44	4.2	0.2488	13.3
	3.09	5.9	0.6852	4.7	2.93	2.9	0.6970	2.7
	7.15	5.3	0.4961	11.1	5.75	3.2	0.5468	3.3
	5.73	3.8	0.5066	4.4	2.24	4.2	0.7110	2.6
	2.59	4.1	0.6494	4.6	7.64	3.5	0.4073	6.0
	1.20	2.6	0.7818	2.4	9.42	3.7	0.3153	10.0
	4.44	2.8	0.6063	3.1	3.22	3.8	0.6929	3.5
	3.77	3.2	0.7029	3.8	3.46	3.6	0.7144	4.2
	8.77	4.3	0.3746	9.6	1.85	6.8	0.7102	6.6
	6.75	6.8	0.4969	12.3	8.29	6.2	0.3871	16.4
	11.27	4.3	0.1871	17.4	8.60	2.8	0.3634	5.9
	13.15	3.6	0.1747	15.3	7.12	4.2	0.4675	6.0
	6.42	4.5	0.4821	6.3	12.03	4.0	0.2581	15.1
	11.91	2.9	0.1451	12.4				
AY-4	$^{238}U/^{206}Pb$	2σ (%)	$^{207}Pb/^{206}Pb$	2σ (%)	$^{238}U/^{206}Pb$	2σ (%)	$^{207}Pb/^{206}Pb$	2σ (%)
	34.59	3.34	0.1204	9.00	36.80	2.73	0.0759	13.86
	29.22	4.86	0.2410	10.53	36.28	3.15	0.0694	10.05
	37.94	3.53	0.1008	9.52	34.91	4.01	0.0860	8.05
	38.18	3.51	0.1091	12.74				

5. Discussion

5.1. Element Variations

A positive correlation between Ag and Mn was found in the Mn–Ag ore (Figures 5 and 6a), indicating that Ag may co-exist in the Mn minerals. Furthermore, there were two types of correlations with respect to Ag and Ba content as shown in Figure 6b. The first tendency showed a positive

correlation between Ag and Ba, indicating Ag may co-exist in a Ba-bearing mineral [32]. This mineral was determined by EPMA to be romanèchite, where a positive correlation between Ag and Ba content was also found (Figure 6d). The second tendency showed no correlation between Ag and Ba (Figure 6b), indicating that another Ag-bearing mineral may occur. This mineral was determined by means of EPMA to be manganite, and a positive correlation between the Ag and K content was found in manganite (Figure 6c).
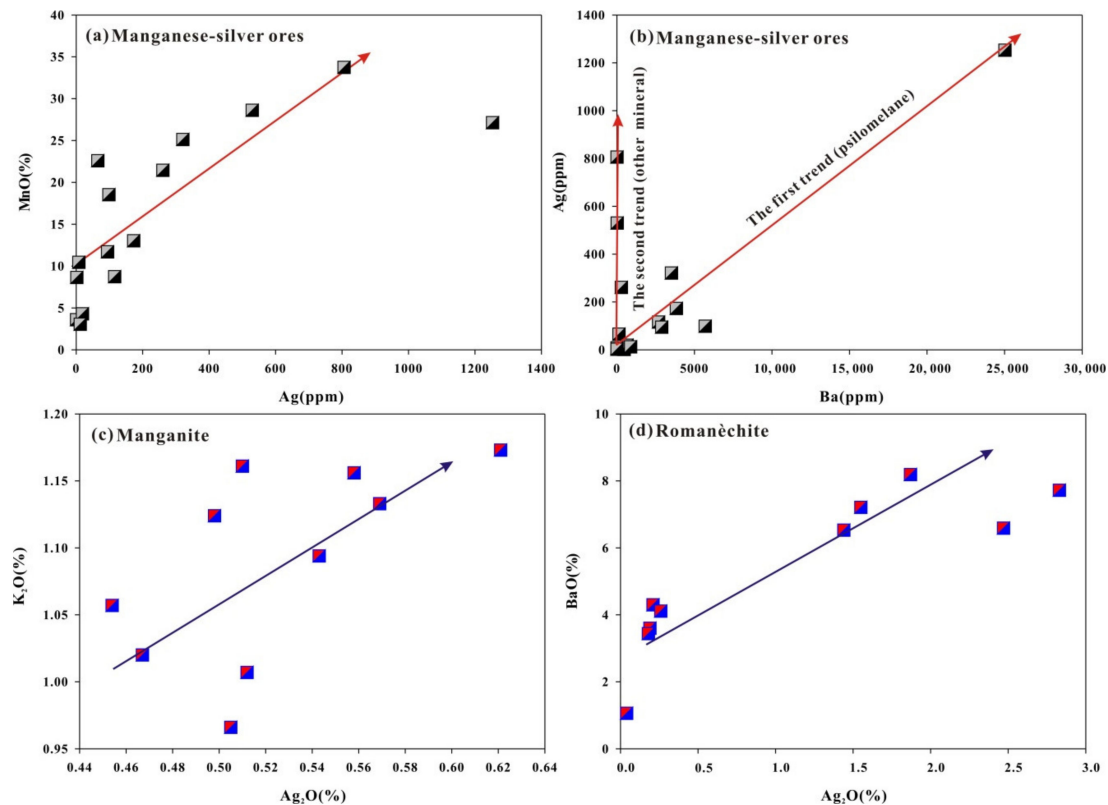
Figure 6. Correlation between Ag and other elements of the Sanbao Mn–Ag ore: (**a**) Ag has a positive correlation with Mn; (**b**) Two types of variation tendencies between Ag and Ba content: first, a positive correlation between Ag and Ba content in a Ba-bearing mineral. Second, Ag content increases while Ba content remains unchanged at a lower level. This tendency shows that another Ag-bearing manganese mineral is Ba-poor; (**c**) A positive correlation between Ag and K content in the pure manganite; (**d**) A positive correlation between Ag and Ba content in the pure romanèchite.

5.2. Occurrence of Ag in Mn Minerals

According to the EPMA results, the major Ag-bearing minerals are manganite and romanèchite.

5.2.1. Manganite

The morphology of manganite is primarily striature (Figure 7a,b), massive (Figure 7c), and acicular (Figure 8a). Manganite in nature is not a homogenous mineral but usually contains a small amount of impurities [33]. Although the total wt.% is less than 100%, the observed data variance between test points is small enough to demonstrate the data's overall reliability (Table 2). Based on average values, this Ag-bearing mineral primarily contains Mn, Fe, K, and Zn, giving an empirical formula of $(Mn_{0.90}Fe_{0.06}K_{0.02}Zn_{0.01})_{\Sigma 0.99}O(OH)$ and the idealized formula $MnO(OH)$ [34].
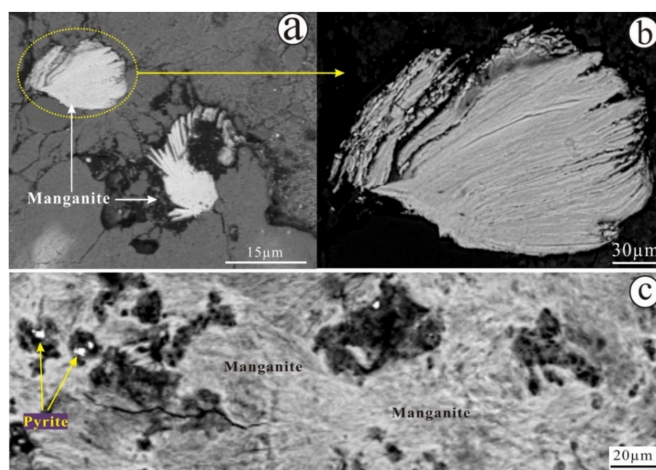
Figure 7. Backscattered electron (BSE) images of the manganite from the Sanbao deposit: (**a**) the exsolution (perthite-like) structure of manganite; (**b**) a larger version of (a); (**c**) relic pyrite associated with massive manganite.

Manganite is formed in conditions of insufficient oxidation [35]. Additionally, cluster crystal manganite is often associated with barite and calcite in a low-temperature vein [36,37]. Some calcite accreted with manganite was found in the Sanbao Mn–Ag deposit. However, manganite generated from sedimentary manganese deposit often becomes massive or oolitic. Manganite from Sanbao is a transitional mineral between Mn^{4+} (e.g., pyrolusite) and Mn^{2+} mineral (e.g., rhodochrosite) [38].

Ag is evenly distributed throughout the Ag-bearing manganite in the deposit. Different geochemical properties of Ag and Mn lead to Ag only occupying a crystal lattice defect instead of replacing Mn in manganite. Furthermore, a positive correlation between Ag and K results from their easy absorption by manganite with a porous texture. Zn occurs in the columnar and dark-fringed manganite (Figure 8b). Columnar manganite contains a small amount of silver and platy manganite does not contain Ag (Figure 9a).
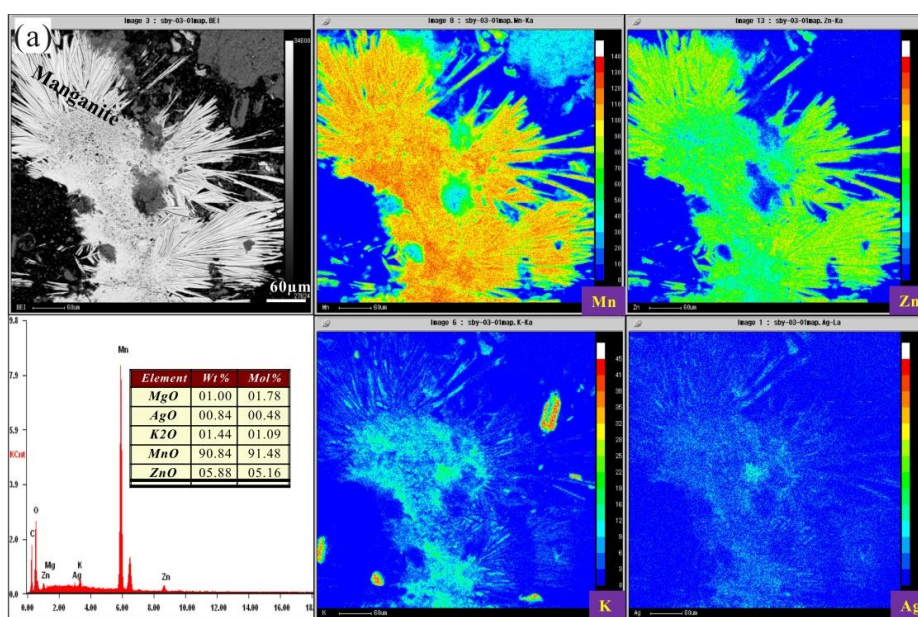

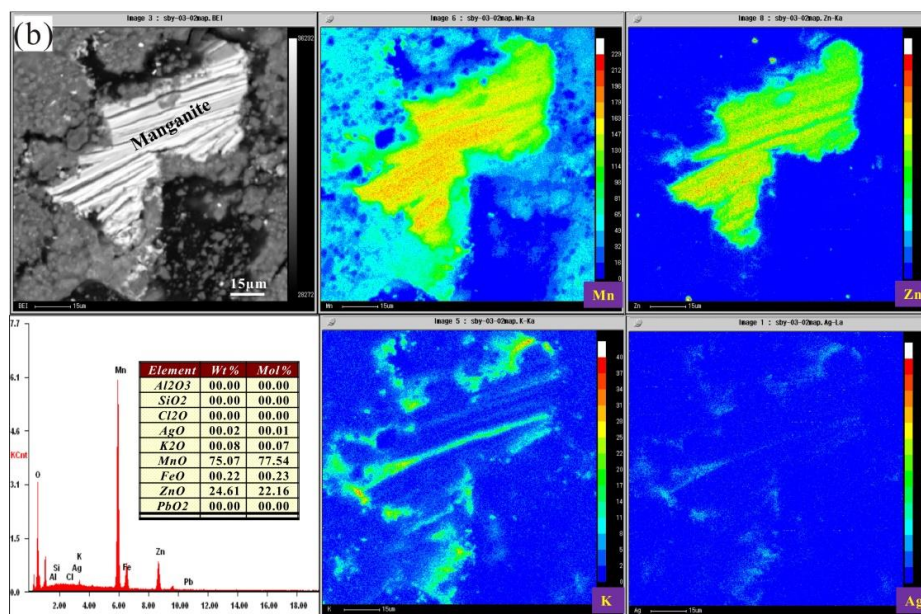| Element	Wt %	Mol %
MgO	01.00	01.78
AgO	00.84	00.48
K2O	01.44	01.09
MnO	90.84	91.48
ZnO	05.88	05.16

Figure 8. *Cont.*

Figure 8. BSE images and the element distributions (WDS, Wavelength Dispersive Spectrometry) of manganite from the Sanbao deposit. (**a**) Manganite with acicular texture often contains high Ag content. Mn and Zn distributions are consistent. Ag distribution is consistent with K distribution. (**b**) Manganite with short columnar texture often contains a small amount of silver. Mn and Zn distributions are consistent in the manganite crystal. Ag distributes along the edge of the manganite. The distribution trends of Ag and K are almost the same in the different types of manganite.
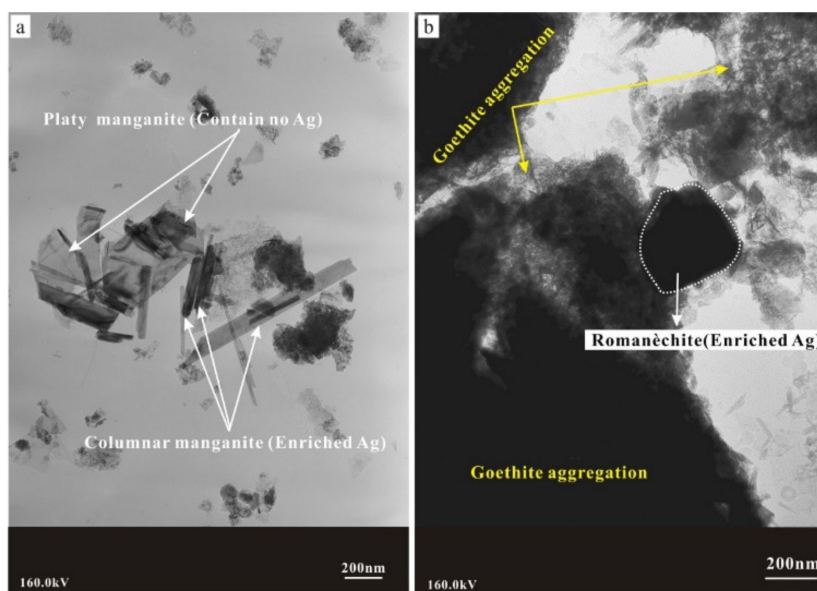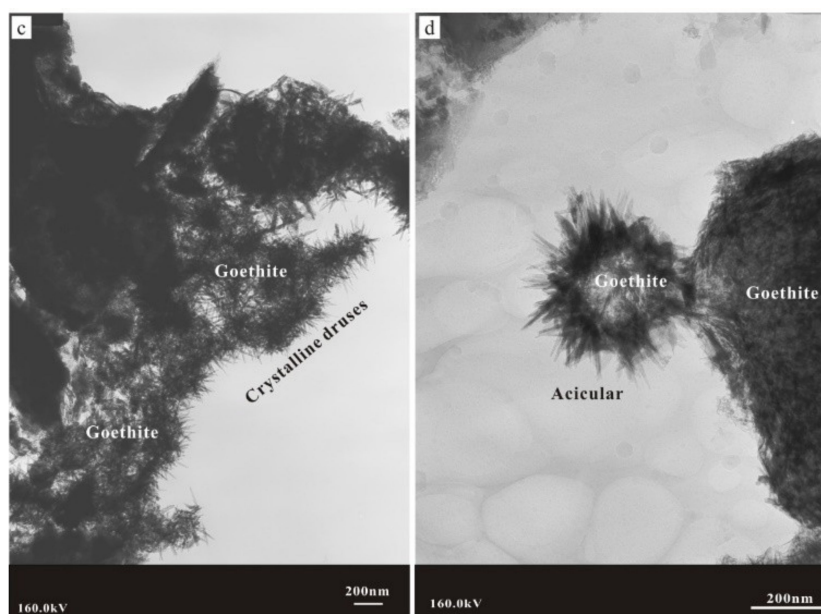

Figure 9. *Cont.*

Figure 9. Three-dimensional surface shape of the oxidized Mn–Ag ore from the Sanbao deposit (transmission electron microscopy): (**a**) columnar manganite contains Ag, whereas platy manganite does not contain Ag; (**b**) Ag-rich romanèchite coexisting with goethite; (**c**) the druse of goethite crystals; (**d**) acicular assemblages of goethite crystals.

5.2.2. Romanèchite

Romanèchite is one of several naturally occurring manganese oxides with a tunnel structure [39,40]. Romanèchite rarely occurs as sizable single crystals, but is intergrown with other minerals, commonly at the unit-cell level [41,42]. Its structure is closely related to those of hollandite and todorokite, and to their many derivative structures [41]. The lower-valence Mn is segregated into the Mn sites at the edges of the triple chains of romanèchite [43,44]. Burns et al. [44] also proposed a similar segregation in the analogous sites of todorokite. Additionally, such an ordering of lower-valence Mn was found for a related material ($Rb_{0.27}MnO_2$) [45]. Structure refinements of some hollandite structures and $Rb_{0.27}MnO_2$ indicate that the lower-valence Mn cation is Mn^{3+} rather than Mn^{2+} [45,46]. If there were no tunnel cations in the manganese oxide tunnel structures, their ideal formula would be $Mn^{4+}O_2$. Based on the above analysis, the MnO is distributed to both Mn^{4+} and Mn^{3+}, and the standardized crystal-chemical formula of romanèchite is defined as $(Ba,H_2O)_2(Mn^{4+},Mn^{3+})_5O_{10}$.

Various forms of romanèchite were observed in the Sanbao Mn–Ag deposit, including idiomorphic (Figure 10a), irregular shape (Figure 10b), colloidal (Figure 10c), and massive (Figure 10d). Ag-rich romanèchite coexisting with goethite was found (Figure 9b). The form of the goethite is crystalline and acicular (Figure 9c,d). Mn is generally replaced by Fe, Al, and V; Ba is replaced by Ca and Na [32,43,47,48]. The hypidiomorphic romanèchite contained sphalerite (Figure 10d). According to the EPMA results (Table 3), the Ag-bearing massive and irregular shape romanèchite primarily contained Mn, Fe, and Ba. The observed wt.% values give a calculated empirical formula $(Ba_{0.18}Ag_{0.05}K_{0.07}Fe_{0.18}(H_2O)_{1.50})_{\Sigma 1.98}(Mn_{0.41}Zn_{0.10}Mn_{3.91}Fe_{0.46}Al_{0.13})_{\Sigma 4.74}O_{10}$, which gives the idealized formula $(Ba,H_2O)_2(Mn^{4+},Mn^{3+})_5O_{10}$.

As seen from the EPMA BSE image, Ag is uniformly distributed in romanèchite with massive texture. Furthermore, independent Ag minerals were not found. Therefore, Ba is replaced by Ag in romanèchite (Figure 11).
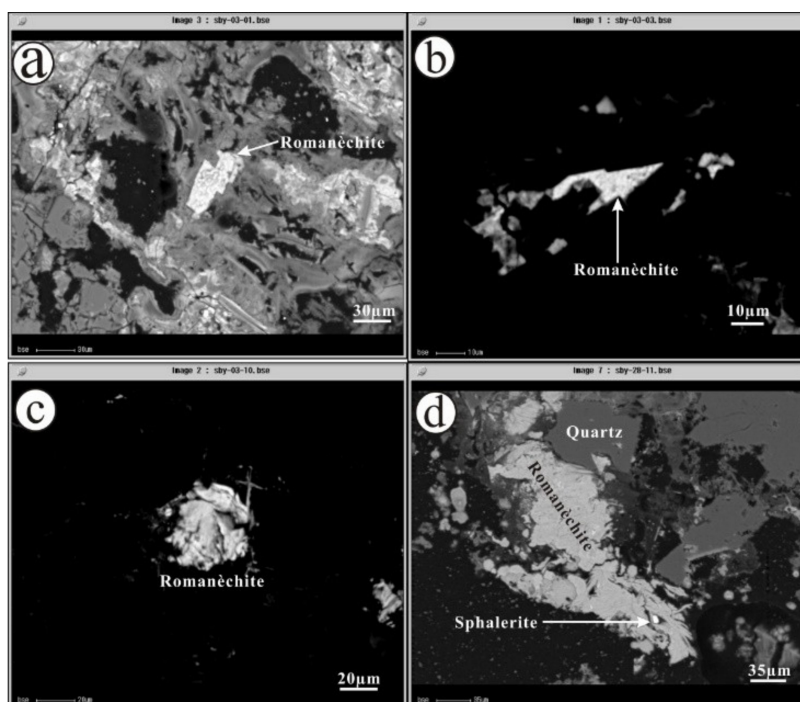
Figure 10. BSE images of romanèchite from the Sanbao deposit: (**a**) single crystal of romanèchite; (**b**) Ag-rich romanèchite; (**c**) colloidal romanèchite with complex composition; (**d**) sphalerite inclusion in romanèchite.
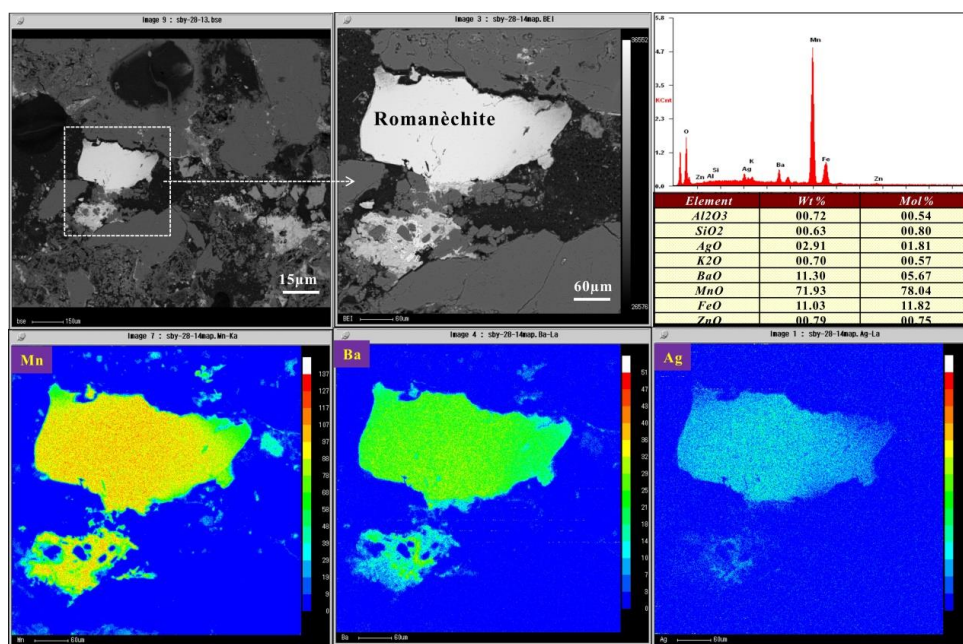

Figure 11. BSE images and element distribution of romanèchite from the Sanbao deposit.

5.3. Geochronology and Ore Genesis

The external standard (AY-4) yielded a Tera–Wasserburg age of 164 ± 12 Ma (Figure 12d), which is consistent with the "standard" age of 158.2 ± 0.4 Ma, within the margin of error [49]. This indicates that the determined age represents true values. The corrected isotopic ratios of the cassiterite sample sby-03 collected from the Sanbao deposit yielded a robust age of 436 ± 17 Ma (Figure 12a–c, Table 6), which is consistent with the age of the Nanwenhe granitic gneiss [10,20,50]. The Xinzhai tin deposit located near

the Sanbao deposit has been dated on cassiterite and yielded an age of 419.1 ± 6.7 Ma [23], which is in agreement with the age of the Sanbao deposit within the range of permitted error. Furthermore, the origin of the Xinzhai tin deposit is closely related to the Caledonian Nanwenhe granitic gneiss [23]. Therefore, the ore genesis of the Sanbao deposit may be related to the Caledonian granitic pluton.
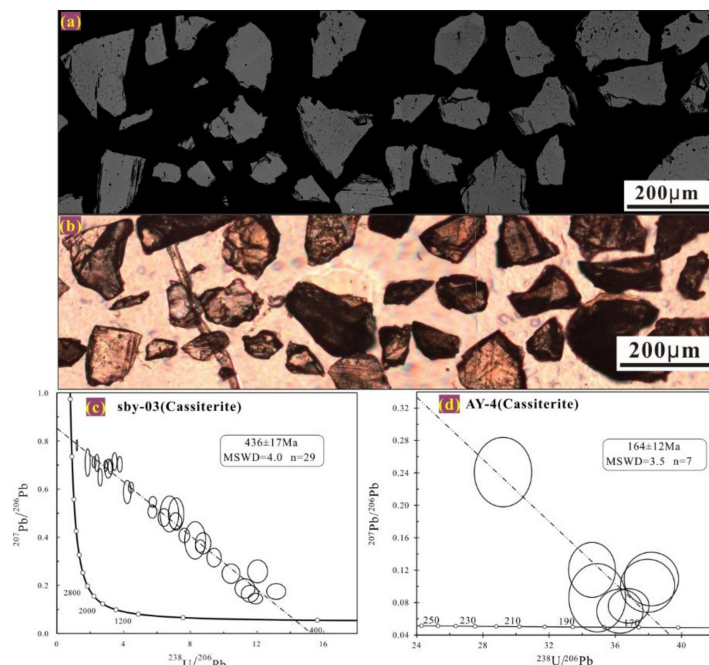

Figure 12. Tera–Wasserburg diagram for the external standard and cassiterite from the Sanbao deposit: (**a**) the BSE image of cassiterite; (**b**) transmitted light of cassiterite; (**c**) Tera–Wasserburg diagram for cassiterite sample sby-03; (**d**) Tera–Wasserburg diagram for the external standard (AY-4).

"Primary ore (rhodochrosite)" and wall rock from the Sanbao Mn–Ag deposit are mainly plotted in the field of fossil Fe–Mn hydrothermal district and of oceanic sediment, respectively (Figure 13, Table 4). The intense positive Eu anomaly of the primary ore is different from the Eu negative anomaly of the wall rock (Figure 14a, Table 5). The La/Ce value (0.51–0.68) of rhodochrosite is near to the hydrothermal sediments value (La/Ce = 1 [51]), but much lower than that measured in sea water (Figure 14b). These results may indicate that primary ore may be of hydrothermal origin rather than sedimentary [52]. In addition, Ag was mainly enriched in the oxidized ore. Accessory minerals, such as cassiterite, rutile and zircon, were also found in the oxidized ore by EPMA.
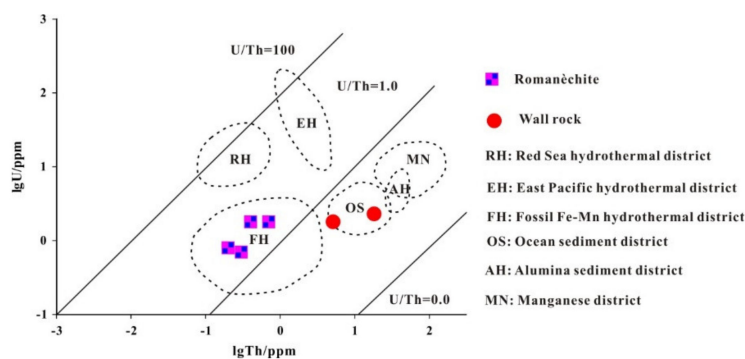

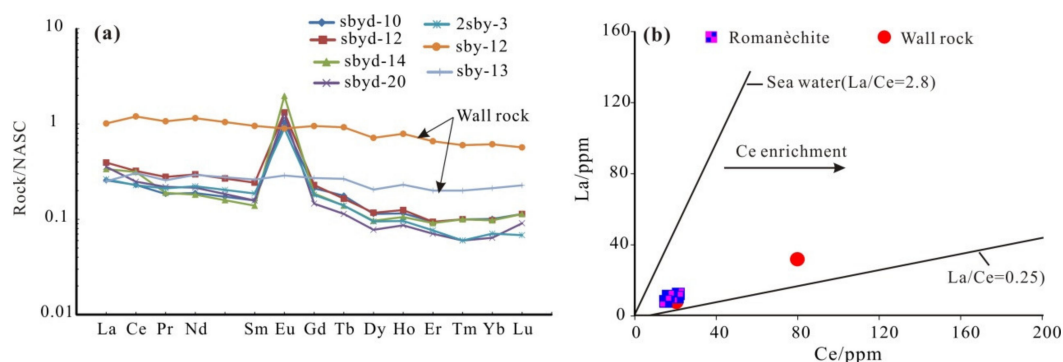**Figure 13.** Trace element characteristics of the Sanbao Mn–Ag ore [53].

Figure 14. REE content of the Sanbao Mn–Ag ore and wall rocks (normalized to the NASC (North American shale composite) values given by [54]): (**a**) REE distribution curves; (**b**) correlation between La and Ce.

5.4. Possible Genetic Model

According to the mineralogy and metallogenesis of the Sanbao Mn–Ag deposit, the current study provides important evidence for collating and stipulating the characteristics of the multi-period and multi-phase petrogenesis-mineralization of Sanbao Mn–Ag ores. The metallogenetic process of the manganese and silver can be divided into four stages: (1) Cambrian: sedimentary strata with a little Ag formed in the Sanbao area, but it has not yet become an economically viable mineral deposit. Thus, the sedimentary strata were treated as an ore source-bed. Additionally, the Tianpeng Formation was an essential part of the sedimentary strata. Rhodochrosite is mainly hosted in the Tianpeng Formation in the Sanbao Mn–Ag deposit (Figure 15a). (2) Cambrian to Silurian: the Tianpeng Formation with a small amount of Ag is favorable ore-source rock and useful ore-preserving wall rock (Table 4). The primary weathering and oxidation of the Tianpeng Formation may supply some ore-forming materials and enrich Ag and Mn. This process contributed directly to forming the oxidized orebody (Figure 15b). Mn exists mainly in the rhodochrosite and manganoan calcite phases in the ore source-bed. Rhodochrosite mineralization contains a small amount of Ag (and base-metals). Mn and Ag are easily leached and enriched through long-term weathering and oxidation (supergene). In the process, most rhodochrosite gradually changed into manganite and romanèchite. As a result, the ore texture became loose and porous and beneficial for Ag entrance. This phenomenon agrees with the fact that Ag primarily occurs in manganite and romanèchite. (3) Silurian: the Caledonian Orogeny is an important tectonic and metallogenetic event in the geological evolution of the Laojunshan ore district [23]. The age of 436 ± 17 Ma, obtained by dating cassiterite from the Mn–Ag ore, is consistent with the emplacement age of the Caledonian Nanwenhe granite and the metallogenic age of the Xinzhai tin deposit [23]. Therefore, the geological evolution and metallogenic dynamics of the Sanbao deposit likely have a close relationship with the Caledonian granite intrusion (Figure 15c). The overprinting from the Caledonian granitic pluton intrusion cannot be ignored [20]. The Ag-rich ore-forming base-metal bearing fluids developed and mineralized along fractures while overprinting the primary and oxidized mineralized layers during the intrusion of granite. The overprinting also drove some Ag into the Mn–Ag ore body. (4) Later Silurian: secondary Ag enrichment (remobilization) occurred during later weathering and oxidation (Figure 15d), eventually evolving into the present Sanbao Mn–Ag deposit.

The above analysis suggests that the Sanbao deposit is characterized by multi-stage mineralization (Figure 15). First, a sedimentary stage occurred during the Cambrian Period and a so-called "primary ore source-bed" formed (Figure 15a) [8]. Second, the primary ore source-bed suffered weathering and oxidation after the Cambrian (Figure 15b). Third, large-scale magma activity occurred at 418–442 Ma (i.e., the Silurian) and produced Caledonian Nanwenhe granite [20]. Ag (with Zn-Pb (Sn)) was further enriched by the overprinting of the Caledonian Nanwenhe granite (Figure 15c). This shows that the Ag mineralization of the Sanbao deposit is likely related to Caledonian Nanwenhe granite rather

than Yanshanian Laojunshan granite [55,56]. Lastly, secondary Ag enrichment occurred during later supergene weathering and oxidation, eventually evolving into the present Sanbao deposit (Figure 15d).
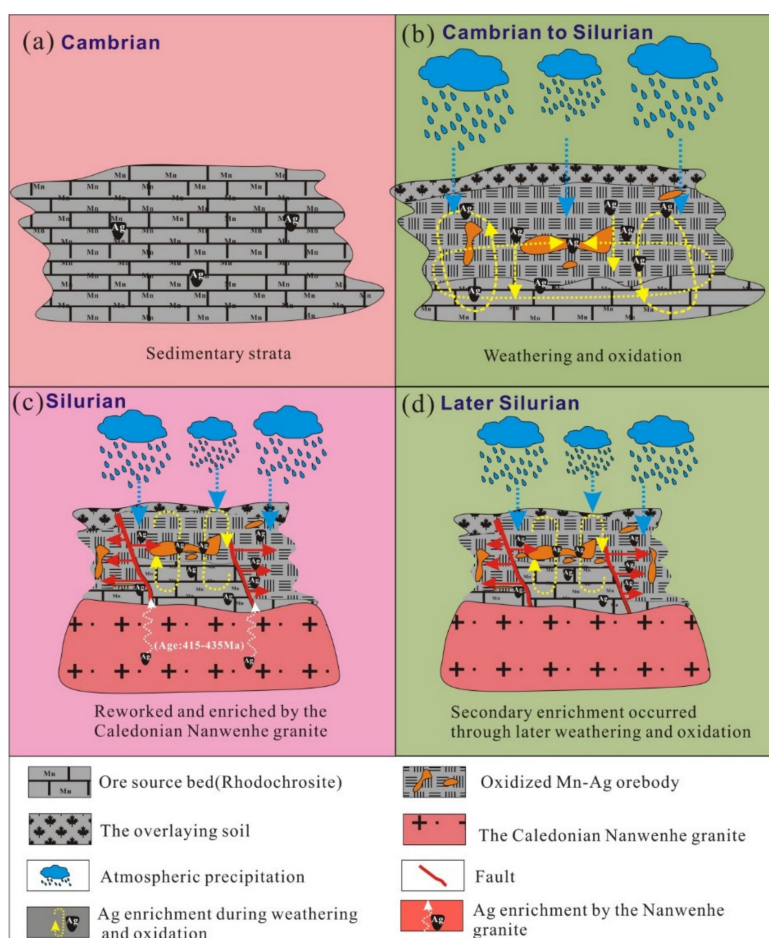

Figure 15. Genesis model of the Sanbao deposit: (**a**) Cambrian: sedimentation stage and ore source-bed started to form; (**b**) Cambrian to Silurian: weathering and oxidation (supergene) of ore body; (**c**) Silurian: the Caledonian magmatism stage on which Ag was enriched by the Nanwenhe granite; (**d**) Later Silurian: secondary Ag enrichment by weathering and oxidation.

6. Conclusions

Based on the results presented in this study, the following conclusions may be drawn:

(1) Manganite and romanèchite are the major Ag-bearing minerals of the Sanbao Mn–Ag deposit. The Ag-bearing manganite primarily contains Mn, Fe, K, and Zn giving an empirical formula of $(Mn_{0.90}Fe_{0.06}K_{0.02}Zn_{0.01})_{\Sigma 0.99}O(OH)$ and the idealized formula $MnO(OH)$. Acicular and columnar manganite contains Ag; the Ag-bearing romanèchite primarily contains Mn, Fe, and Ba. The observed wt.% values give a calculated empirical formula $(Ba_{0.18}Ag_{0.05}K_{0.07}Fe_{0.18}(H_2O)_{1.50})_{\Sigma 1.98}(Mn_{0.41}Zn_{0.10}Mn_{3.91}Fe_{0.46}Al_{0.13})_{\Sigma 4.74}O_{10}$, which gives the idealized formula $(Ba,H_2O)_2(Mn^{4+},Mn^{3+})_5O_{10}$. Ba is replaced by Ag in romanèchite.

(2) The corrected isotopic ratios of the cassiterite sample sby-03 collected from the Sanbao deposit yielded an age of 436 ± 17 Ma, which is consistent with the age of the Nanwenhe granitic gneiss and the mineralization age of the Xinzhai tin deposit in the Laojunshan ore district. The origin of the Xinzhai tin deposit is closely related to the Caledonian Nanwenhe granitic gneiss. This therefore implied that the ore genesis of the Sanbao deposit may be related to the Caledonian granitic pluton. Combined with other geochemical proxies (Zn-Pb (Sn)), the primary Sanbao Mn–Ag deposit may be of magmatic hydrothermal origin (skarn-related) rather than sedimentary.

(3) Based on newly obtained data on mineralogy and metallogeny of the Sanbao deposits, a possible genetic model is established. Firstly, the so-called "primary ore source-bed" formed in the Cambrian. Secondly, the primary ore source-bed suffered weathering and oxidation after the Cambrian. Thirdly, large-scale magma activity occurred at 418–442 Ma (i.e., the Silurian) and produced Caledonian Nanwenhe granite. Ag (with Zn–Pb (Sn)) was further enriched by the overprinting of the Caledonian Nanwenhe granite. Lastly, secondary Ag enrichment occurred during later supergene weathering and oxidation, eventually evolving into the present Sanbao deposit.

Author Contributions: Conceptualization, H.W. and S.D.; Methodology, S.L.; Investigation, C.Q. and G.Y.; Resources, Y.Y.; Data Curation, P.F.; Writing—Original Draft Preparation, S.D.; Writing—Review & Editing, S.D. and H.W. All authors have read and agreed to the published version of the manuscript.

Conflicts of Interest: The authors declare no conflicts of interest.

References

1. Costagliola, P.; Di Benedetto, F.; Benvenuti, M.; Bernardini, G.P.; Cipriani, C.; Lattanzi, P.F.; Romanelli, M. Chemical speciation of Ag in galena by EPR spectroscopy. *Am. Mineral.* **2004**, *88*, 1345–1350. [CrossRef]

2. Gammons, C.H.; Barnes, H. The solubility of Ag_2S in near-neutral aqueous sulfide solutions at 25 to 300 °C. *Geochim. Cosmochim. Acta* **1989**, *53*, 279–290. [CrossRef]

3. Renders, P.; Seward, T. The stability of hydrosulphido-and sulphido-complexes of Au (I) and Ag (I) at 25 °C. *Geochim. Cosmochim. Acta* **1989**, *53*, 245–253. [CrossRef]

4. Stefánsson, A.; Seward, T. Experimental determination of the stability and stoichiometry of sulphide complexes of silver (I) in hydrothermal solutions to 400 °C. *Geochim. Cosmochim. Acta* **2003**, *67*, 1395–1413.

5. Wang, J. A study of occurrences of Ag in Pb-Zn-Cu Ore deposits in China. *Acta Geol. Sin.* **2010**, *4*, 516–520.

6. Zhang, X.-Y.; Tian, X.-D.; Zhang, D.-F. Separation of silver from manganese-silver ore with cellulose as reductant. *Trans. Nonferr. Met. Soc. China* **2006**, *16*, 705–708. [CrossRef]

7. Sharp, T.G.; Buseck, P.R. The distribution of Ag and Sb in galena; inclusions versus solid solution. *Am. Mineral.* **1993**, *78*, 85–95.

8. Jia, F.J. Researches on Metallogenic Series and Metallogenic Regularities in Laojunshan Metallogenic Belt, Yunnan Province. Ph.D. Thesis, Kunming University of Science and Technology, Kunming, China, 2010; pp. 1–105. (In Chinese).

9. Yang, G.N.; Gong, H.B. The ore composition of Sanbao Malipo Ag multimetallic deposit and a discussion about the genesis. *Yunnan Geol.* **2009**, *28*, 60–66, (In Chinese with English abstract).

10. Feng, J.R. The Ore-Forming Fluid and Metallogenesis of Nanyangtian Tungsten Deposit in Malipo, Yunnan Province, China. Ph.D. Thesis, Chinese Academy of Geological Sciences, Beijing, China, 2011; pp. 1–111. (In Chinese).

11. Hu, R.Z.; Chen, W.T.; Xu, D.R.; Zhou, M.F. Reviews and new metallogenic models of mineral deposits in south China: An introduction. *J. Asian Earth Sci.* **2017**, *137*, 1–8. [CrossRef]

12. Yao, J.L.; Shu, L.S.; Cawood, P.A.; Li, J.Y. Delineating and characterizing the boundary of the Cathaysia Block and the Jiangnan orogenic belt in South China. *Precambrian Res.* **2016**, *275*, 265–277. [CrossRef]

13. Faure, M.; Ishida, K. The Mid-Upper Jurassic olistostrome of the west Philippines: A distinctive key-marker for the North Palawan block. *J. Southeast Asian Earth Sci.* **1990**, *4*, 61–67. [CrossRef]

14. Wang, Y.J.; Fan, W.M.; Sun, M.; Liang, X.; Zhang, Y. Geochronological, geochemical and geothermal constraints on petrogenesis of the Indosinian peraluminous granites in the South China Block: A case study in the Hunan Province. *Lithos* **2007**, *96*, 475–502. [CrossRef]

15. Zhou, M.F.; Zhao, J.H.; Qi, L. Zircon U-Pb geochronology and elemental and Sr-Nd isotopic geochemistry of Permian mafic rocks in the Funing area, SW China. *Contrib. Mineral. Petrol.* **2006**, *151*, 1–19. [CrossRef]

16. Zhou, M.F.; Yan, D.P.; Kennedy, A.K.; Li, Y.; Ding, J. SHRIMP U-Pb zircon geochronological and geochemical evidence for Neoproterozoic arc-magmatism along the western margin of the Yangtze Block, South China. *Earth Planet Sci. Lett.* **2002**, *196*, 51–67. [CrossRef]

17. Zhou, M.F.; Zhao, X.F.; Chen, W.T.; Li, X.C.; Wang, W.; Yan, D.P.; Qiu, H.N. Proterozoic Fe–Cu metallogeny and supercontinental cycles of the southwestern Yangtze Block, Southern China and Northern Vietnam. *Earth Sci. Rev.* **2014**, *139*, 59–82. [CrossRef]

18. Yan, D.P.; Zhou, M.F.; Song, H.L.; Wang, X.W.; Malpas, J. Origin and tectonic significance of a Mesozoic multi-layer over-thrust within the Yangtze Block (South China). *Tectonophysics* **2003**, *361*, 239–254. [CrossRef]

19. Yu, J.H.; Zhou, X.; O'Reilly, S.Y.; Zhao, L.; Griffin, W.L.; Wang, R.; Wang, L.; Chen, X. Formation history and protolith characteristics of granulite facies metamorphic rock in Central Cathaysia deduced from U-Pb and Lu–Hf isotopic studies of single zircon grains. *Chin. Sci. Bull.* **2005**, *50*, 2080–2089. [CrossRef]

20. Guo, L.; Liu, Y.; Li, C.; Xu, W.; Ye, L. SHRIMP zircon U-Pb geochronology and lithogeochemistry of Caledonian Granites from the Laojunshan area, Southeastern Yunnan province, China: Implications for the collision between the Yangtze and Cathaysia blocks. *Geochem. J.* **2009**, *43*, 101–122. [CrossRef]

21. Mei, Y.X.; Pei, R.F.; Yang, D.F.; Dai, Z.X.; Li, J.W.; Xu, C.R.; Qu, H.Y. Global metallogenic domains and districts. *Miner. Depos.* **2009**, *4*, 383–389, (In Chinese with English abstract).

22. Tu, G.C.; Gao, Z.M.; Hu, R.Z.; Zhang, Q.; Li, C.Y.; Zhao, Z.H.; Zhang, B.G. *Geochemistry and Mineralization Mechanism of Dispersed Elements*; Geology Publishing House: Beijing, China, 2003; pp. 1–424. (In Chinese)

23. Du, S.J.; Wen, H.J.; Qin, C.J.; Yan, Y.F.; Yang, G.S.; Fan, H.F.; Zhang, W.J.; Zhang, L.; Wang, D.; Li, H.M. Caledonian ore-forming event in the Laojunshan mining district, SE Yunnan Province, China: In-Situ LA-MC-ICP-MS U-Pb dating on cassiterite. *Geochem. J.* **2015**, *49*, 11–22. [CrossRef]

24. Wang, X.K. Geological-Geochemical characteristics of Xinzhai tin deposit in Malipo. *Geol. Yunnan* **1994**, *13*, 1–16, (In Chinese with English abstract).

25. Qi, L.; Hu, J.; Gregoire, D.C. Determination of trace elements in granites by inductively coupled plasma mass spectrometry. *Talanta* **2000**, *51*, 507–513.

26. Tan, Q.P.; Xia, Y.; Xie, Z.J.; Yan, J. Migration paths and precipitation mechanisms of ore-forming fluids at the Shuiyindong Carlin-type gold deposit, Guizhou, China. *Ore Geol. Rev.* **2015**, *69*, 140–156. [CrossRef]

27. Chen, X.C.; Hu, R.Z.; Bi, X.W.; Li, H.M.; Lan, J.B.; Zhao, C.H.; Zhu, J.J. Cassiterite LA-MC-ICP-MS U/Pb and muscovite [40]Ar/[39]Ar dating of tin deposits in the Tengchong-Lianghe tin district, NW Yunnan, China. *Miner. Depos.* **2014**, *49*, 843–860. [CrossRef]

28. Gulson, B.L.; Jones, M.T. Cassiterite: Potential for direct dating of mineral deposits and a precise age for the Bushveld Complex granites. *Geology* **1992**, *20*, 355–358. [CrossRef]

29. Yuan, S.; Peng, J.; Hu, R.; Li, H.; Shen, N.; Zhang, D. A precise U–Pb age on cassiterite from the Xianghualing tin-polymetallic deposit (Hunan, South China). *Miner. Depos.* **2008**, *43*, 375–382. [CrossRef]

30. Wang, Z.Q.; Chen, B.; Ma, X.H. In-Situ LA-ICP-MS U-Pb age and geochemical data of cassiterite of the Furong tin deposit, the Nanling Range: Implications for the origin and evolution of the ore-forming fluid. *Chin. Sci. Bull.* **2014**, *59*, 2505–2519, (In Chinese with English abstract).

31. Ludwig, K. *User's Manual for Isoplot/Ex v. 2.47. A Geochronological Toolkit for Microsoft Excel*; BGC Special Publication; Berkeley Geochronological Center: Berkeley, CA, USA, 2001.

32. Tebano, A.; Balestrino, G.; Boggio, N.; Aruta, C.; Davidson, B.; Medaglia, P. High-Quality in-situ manganite thin films by pulsed laser deposition at low background pressures. *Eur. Phys. J. B-Condens. Matter Complex Syst.* **2006**, *51*, 337–340. [CrossRef]

33. Hewett, D.F. Manganite, hausmannite, braunite; features, modes of origin. *Econ. Geol.* **1972**, *67*, 83–102. [CrossRef]

34. Fan, D.; Yang, P. Introduction to and classification of manganese deposits of China. *Ore Geol. Rev.* **1999**, *15*, 1–13. [CrossRef]

35. Luo, Y.; Li, S,; Tan, W.F.; Liu, F.; Cai, C.F.; Qiu, G.H. Oxidation process of dissolvable sulfide by manganite and its influencing factors. *Environ. Sci.* **2016**, *37*, 1539–1545, (In Chinese with English abstract).

36. Xiao, Q.H.; Hui, W.D.; Qin, K.Z. Genetic types and exploration direction of manganese deposits in Dashui Mn ore belt on northern margin of Central Tianshan, eastern Xinjiang. *Miner. Depos.* **2007**, *26*, 89–97. (In Chinese with English abstract)

37. He, Z.W.; Yang, R.D.; Gao, J.B.; Cheng, W.; Wen, G.G. The structure character of manganese ore deposit of datangpo-period of neoproterozoic in Songtao of Guizhou. *China's Manganese Ind.* **2013**, *31*, 5–8. (In Chinese with English abstract)

38. Huang, J.S.; Zhu, K.J.; Wang, S.B.; Zhu, Z.S. Outline of marine Mn deposits in the South China. *Contrib. Geol. Miner. Resouces Res.* **1996**, *3*, 9–17, (In Chinese with English abstract).

39. Hey, M.H. International mineralogical association: Commission on new minerals and mineral names. *Mineral. Mag.* **1982**, *46*, 513–514. [CrossRef]

40. Turner, S.; Post, J.E. Refinement of the substructure and superstructure of romanèchite. *Am. Mineral.* **1988**, *73*, 1155–1161.

41. Turner, S.; Buseck, P.R. Manganese oxide tunnel structures and their intergrowths. *Science* **1979**, *203*, 456–458. [CrossRef]

42. Giovanoli, R.; Balmer, B. Darstellung und Reaktionen von Psilomelan(Romanechit) $Ba_2Mn_{15}O_{30} \cdot 4H_2O$. *Chimia* **1983**, *37*, 424–427.

43. Wadsley, A.D. The crystal structure of psilomelane$(Ba,H_2O)_2Mn_5O_{10}$. *Acta Crystallogr.* **1953**, *6*, 433–438. [CrossRef]

44. Burns, R.G.; Burns, V.M.; Stockman, H.W. A review of the todorokite-buserite problem: Implications to the mineralogy of marine manganese nodules. *Am. Mineral.* **1983**, *68*, 972–980.

45. Tamada, O.; Yamamoto, N. The crystal structure of a new manganese dioxide $(Rb_{0.27}TMnO_2)$ with a giant tunnel. *Mineral. J.* **1986**, *13*, 130–140. [CrossRef]

46. Post, J.E.; Von Dreele, R.B.; Buseck, P.R. Symmetry and cation displacements in hollandites: Structure refinements of hollandite, cryptomelane and priderite. *Acta Crystallogr.* **1982**, *38*, 1056–1065. [CrossRef]

47. Roy, S. Mineralogy of the different genetic types of manganese deposits. *Econ. Geol.* **1968**, *63*, 760–786. [CrossRef]

48. Zhao, S.R.; Bian, Q.J.; Ling, Q.C. *The Crystallography and Mineralogy*; Higher Education Press: Beijing, China, 2004; pp. 1–441. (In Chinese)

49. Yuan, S.; Peng, J.; Hao, S.; Li, H.; Geng, J.; Zhang, D. In-Situ LA-MC-ICP-MS and ID-TIMS U–Pb geochronology of cassiterite in the giant Furong tin deposit, Hunan Province, South China: New constraints on the timing of tin–polymetallic mineralization. *Ore Geol. Rev.* **2011**, *43*, 235–242. [CrossRef]

50. Tan, H.Q.; Liu, Y.P.; Xu, W.; Guo, L.G.; Ye, L.; Li, C.Y. A Study on SHRIMP and TIMS zircons dating on low-to medium-grade ortho-metamorphic rocks: Example on the Nanwenhe granitic gneiss, Southeastern Yunnan Province, China. *Acta Mineral. Sin.* **2011**, *31*, 62–69, (In Chinese with English abstract).

51. Hogdahl, O.; Melsom, S.; Bowen, V.T. Neutron activation analysis of lanthanide elements in sea water. *Adv. Chem. Ser.* **1968**, *73*, 308–325.

52. Boström, K. Genesis of ferromanganese deposits-diagnostic criteria for recent and old deposits. In *Hydrothermal Processes at Seafloor Spreading Centers*; Plenum Press: New York, NY, USA, 1983; pp. 473–489.

53. Toth, J.R. Deposition of submarine crusts rich in manganese and iron. *Geol. Soc. Am. Bull.* **1980**, *91*, 44–54. [CrossRef]

54. McLennan, S. Rare earth elements in sedimentary rocks; influence of provenance and sedimentary processes. *Rev. Mineral. Geochem.* **1989**, *21*, 169–200.

55. Li, K.W.; Zhang, Q.; Wang, D.P.; Cai, Y.; Liu, Y.P. LA-MC-ICP-MS U-Pb Geochronology of Cassiterite from the Bainiuchang Polymetallic Deposit, Yunnan Province, China. *Acta Mieral. Sin.* **2013**, *33*, 203–209. (In Chinese with English abstract)

56. Xu, B.; Jiang, S.Y.; Wang, R.; Ma, L.; Zhao, K.D.; Yan, X. Late Cretaceous granites from the giant Dulong Sn-polymetallic ore district in Yunnan Province, South China: Geochronology, geochemistry, mineral chemistry and Nd–Hf isotopic compositions. *Lithos* **2015**, *218*, 54–72. [CrossRef]